EMF-Aware Probabilistic Shaping Design for Hardware Distorted Communication Systems

Sidrah Javed [1,*], Ahmed Elzanaty [2], Osama Amin [1], Mohamed-Slim Alouini [1] and Basem Shihada [1]

[1] *CEMSE Division, King Abdullah University of Science and Technology (KAUST), Thuwal, Makkah Province, Saudi Arabia*
[2] *Institute for Communication Systems (ICS), University of Surrey, Guildford GU2 7XH, U.K.*

Correspondence*:
Corresponding Author
sidrah.javed@kaust.edu.sa

ABSTRACT

The fifth-generation cellular network requires dense installation of radio base stations (BS) to support ever-increasing demands of high throughput and coverage. The ongoing deployment has triggered some health concerns among the community. To address this uncertainty, we propose an EMF-aware probabilistic shaping design for hardware distorted communication systems. The proposed scheme aims to minimize human exposure to radio-frequency (RF) radiations while achieving the target throughput using probabilistic shaping. The joint optimization of the transmit power and non-uniform symbol probabilities is a non-convex optimization problem. Therefore, we employ alternate optimization and successive convex approximation to solve the subsequent problems. Our findings reveal a significant reduction in the users' exposure to EMF while achieving the requisite quality-of-service with the help of probabilistic shaping in a hardware distorted communication system.

Keywords: Asymmetric signaling, Error probability analysis, Hardware impairments, Improper noise, Non-uniform probabilities, Radiation exposure

1 INTRODUCTION

The next-generation wireless communication networks are expected to fulfill the ever-increasing demands of higher data rates, ultra-reliability, minimal latency, high energy efficiency, and massive connectivity for many users/devices (Latva-aho et al. (2020)). The fifth-generation (5G) is envisioned to support numerous diverse services, such as enhanced mobile broadband (eMBB), ultra-reliable low latency communication (URLLC) and massive machine-type communication (mMTC) (Wan et al. (2018)). Some of the new spectrum allocated for 5G deployments, e.g., millimeter waves, suffers from relatively high path loss limiting the coverage area. Thus, network densification becomes essential to achieve the promised data rate, which can be realized over space (e.g., dense deployment of base station (BS)s in small cells) and frequency (large segments of RF spectrum in diverse bands) (Bhushan et al. (2014)).

Installation of the 5G cellular technology with extreme node and network densification (with BSs being closer to users) is raising health concerns about the impact of electric and magnetic fields (EMF) exposure on the population. These worries have sparked several protests against 5G technology and led to some attacks on the 5G BSs (Elzanaty et al. (2021)). Recently, anti-5G protests were held in 30 countries around the world against the threat of 5G wireless technology to public health, the environment, and privacy.

Indeed, the thermal effect is the only proven health impact from the RF non-ionized short-term exposure. Therefore, it is necessary to keep the radiation intensity below specific values defined by the exposure regulations and guidelines, e.g., Federal Communications Commission (FCC) and International Commission on Non-Ionizing Radiation Protection (ICNIRP) (Buchner and Rivasi (2020)). Nevertheless, there is a debate about the severe health impacts due to long-term exposure to EMF (National Toxicology Program (2018b,a); Vornoli et al. (2019)). Hence, the International Agency for Research on Cancer (IARC) classified RF radiation as "possibly carcinogenic to humans" (Vornoli et al. (2019); Group (2013); Wilbourn et al. (1986)).

Recently, a comprehensive study revealed that the exposure due to the uplink (UL) from the user equipment (UE) is higher than that from the BS due to the proximity of the UE to the user (Lou et al. (2021)). Another work has proposed an architectural solution to minimize the EMF exposure using Reconfigurable intelligent surfaces (Ibraiwish et al. (2022)). Further study is focused on the meticulous cellular network planning to limit the exposure from BSs exploiting MIMO while ensuring coverage and capacity constraints (Matalatala et al. (2018)). From regulatory aspects, some possible risk mitigation strategies are the dismission of legacy 2G/3G/4G technologies and reduction of emission from non-cellular sources (Chiaraviglio et al. (2021)).

Nevertheless, as mentioned earlier, the EMF exposure-based research does not consider any hardware impairments, which can drastically affect the system performance, such as raising the noise floor. For instance, in order to reach the target data rates in eMBB, the hardware distortion (HWD) should be mitigated. Generally, the user will send much higher power, escalating their RF exposure, to achieve the target rate. The users may still not reach the required throughput due to the saturation for the data rate at higher SNR as the distortion noise increases with the transmit power.

HWD requires some meticulously designed systems to compensate for its effect and mitigate the performance loss. improper Gaussian signaling (IGS) is an effective compensation signaling scheme that can alleviate the impact of several interference and imperfection sources (Javed et al. (2019)). However, realizing the IGS comes with the inherent problems of unbounded peak-to-average power ratio and high detection complexity (Santamaria et al. (2018); Javed et al. (2020)). As a consequence, researchers employ finite discrete asymmetric signaling (AS) schemes that can be achieved by geometric shaping (GS), probabilistic shaping (PS), or hybrid shaping (HS) (Elzanaty and Alouini (2022); Javed et al. (2021)). In this work, we propose an asymmetric signaling by adopting PS to tackle improper HWD and minimize EMF exposure to the users while maintaining throughput quality of service (QoS). The contributions of this paper are summarized as follows:

- We model HWD and EMF exposure in the next generation wireless cellular network. We present appropriate receiver and rigorous error probability analysis considering the improper distortion noise.
- We propose probability shaping as a form of asymmetric signaling to effectively mitigate improper HWDs and reduce EMF exposure while maintaining QoS in terms of user throughput.
- We employ alternate optimization to jointly design the transmit power of users and non-uniform symbol probabilities. We further use the successive convex approximation and the Newton-Raphson method to solve the subsequent problems.

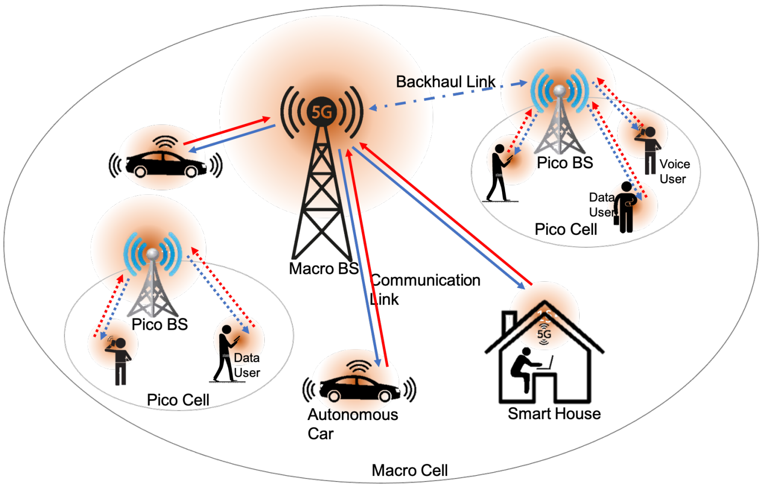

Figure 1. EMF Exposure from 5G Network Infrastructure

The rest of the paper is organized such that Section 2 illustrates the system description and adopted models to characterize the radiation exposure and HWD. Error probability analysis is carried out in Section 3, whereas Section 4 covers the problem formulation and optimization framework. Numerical results are presented in Section 5, followed by the conclusion in Section 6.

2 SYSTEM DESCRIPTION

In this section, we quantify the EMF-exposure of the human population in a next-generation wireless cellular communication system. The network comprises of macro-cell with a macro BS and multiple pico-cells with their serving pico BSs. Apart from the transmitting radiations from the BSs in downlink (DL), we are interested in the EMF exposure caused by the handheld devices. For instance, the RF radiations emitting from the cell phones and smart watches are stronger near the users resulting in the near-field exposure, whereas the EMF transmission density from BS towers resides far from the users rendering far-field exposure. Likewise, increasing applications and use cases including but not limited to autonomous vehicles and smart homes/offices, etc., are extending the radiation footprint near humans. Figure 1 demonstrates a strong radiation pattern near users in the case of voice users compared to data users. In addition, we account for the performance degradation caused by the additive HWDs accumulating from various blocks in non-ideal RF transceivers. We propose a generalized digital communication system capable of transmitting non-uniformly distributed symbols (from a uniform bitstream using distribution matching) while employing an appropriate receiver for optimal detection.

2.1 Radiation Exposure

The modeling and quantification of human exposure in a wireless cellular network are critical to facilitate the reduction efforts. Numerous studies have identified the essential parameters influencing this end exposure (Kuehn et al. (2019); Lou et al. (2021); Vermeeren et al. (2015a)). The EMF exposure, quantified as Exposure Index (EI), is primarily dictated by the network topology, environment, radio access technology, user scenarios, and service types, etc. (Kuehn et al. (2019)). The EI can be written as the weighted sum of all branches in the chain of exposure (Lou et al. (2021))

$$\mathrm{EI} = \sum_{g} \sum_{p} \sum_{e} \sum_{r} \sum_{l} \sum_{s} f\left(\mathrm{SAR}^{\mathrm{UL}}, \alpha, \mathrm{SAR}^{\mathrm{DL}}, \varrho\right) \tag{1}$$

where specific absorption rate (SAR), measured in W/Kg, is the power absorbed per mass of the exposed tissue for a given period with $\mathrm{SAR}^{\mathrm{UL}}$ and $\mathrm{SAR}^{\mathrm{DL}}$ indicating the normalized values of the UL and DL induced SAR when the mean transmit power $\alpha = 1\mathrm{W}$ and the mean received power density $\varrho = 1\mathrm{W}/\mathrm{m}^2$, respectively. The EI is integrated over different age groups g (e.g., children, young people, adults, and seniors), user posture p (e.g., standing, sitting), environments e (e.g., indoor, outdoor, commuting), radio access technology r (e.g., GSM, UMTS, WiFi, 5G), layers l (macro, micro, pico, femto), service/usage type s (e.g., voice and data) (Tesanovic et al. (2014)). We consider an exposure scenario of the next-generation cellular network in an indoor environment where the reference SAR is averaged over different population ages and postures, accommodating both data and voice usage types. The EI for both UL and DL can be given by $\mathrm{EI} = \mathrm{EI}^{\mathrm{UL}} + \mathrm{EI}^{\mathrm{DL}}$, combining the DL exposure induced all day long by base stations/access points and the UL exposure incurred by individual wireless communication devices.

Contrary to the general perception, the SAR from UL renders the dominant part instead of the one from DL with low ϱ (generally $\leq 10\mathrm{mW}/\mathrm{m}^2$ according to FCC) given a significant distance between the transmitter and receiver. Thus, the exposure index (EI) metric in the presented scenario is dominated by the UL as $\mathrm{EI}(\alpha) = \mathrm{SAR}^{\mathrm{UL}}\alpha$, the reference whole body or localized SAR mainly depends on the required service and the posture (Vermeeren et al. (2015b); Lou et al. (2021)).

2.2 Hardware Impaired Signal Model

Non-linear transfer functions of various transmitter RF stages, such as digital-to-analog converter, band-pass filter, and high power amplifier, resulting in additive distortion noise η_{t}, which is distributed as a zero-mean complex Gaussian random variable $\eta_{\mathrm{t}} \sim \mathcal{CN}(0, \kappa_{\mathrm{t}}, \tilde{\kappa}_{\mathrm{t}})$ with variance κ_{t} and pseudo-variance $\tilde{\kappa}_{\mathrm{t}}$. The complete statistical characterization requires pseudo-variance, in addition to the variance, accounting for the correlated and/or unequal power distribution among quadrature components of the general complex Gaussian random variable (Javed et al. (2017)). Importantly, the value of pseudo-variance is limited by the variance as $|\tilde{\kappa}_{\mathrm{t}}| \leq \kappa_{\mathrm{t}}$ (Björnson et al. (2013); Schenk (2008)).

The Gaussian model for the aggregate residual RF distortions is based on various theoretical investigations, including the central limit theorem and measurement results after applying existing compensation schemes (Wenk (2010); Zetterberg (2011); Boulogeorgos et al. (2016); Xia et al. (2015); Suzuki et al. (2008); Studer et al. (2010); Duy et al. (2015); Björnson et al. (2014) and references therein). This can also be motivated analytically by the central limit theorem. The accumulative distortions raise the noise floor of the transmitted signal as $x_{\mathrm{tx}} = x_m + \eta_{\mathrm{t}}$, where x_m is the single-carrier band-pass modulated signal taken from M-ary QAM, M-ary PSK, or M-ary PAM constellation with a probability mass function $p_m \triangleq p_X(x_m)$, rendering the transmission probability of symbol x_m, and $\mathbf{p} \triangleq [p_1, p_2, \cdots, p_M]$. Let us define the set that includes all possible symbol distributions as

$$\mathbb{S} = \left\{ \mathbf{p} : \mathbf{p} = [p_1, p_2, \cdots, p_M], \sum_{j=1}^{M} p_j = 1, p_j \geq 0, \forall j \in \{1, 2, \cdots, M\} \right\}.$$

The information-bearing signal is transmitted with average power α and received under additive white Gaussian noise (AWGN) condition and receiver distortions $\eta_{\mathrm{r}} \sim \mathcal{CN}(0, \alpha\,\kappa_{\mathrm{r}}, \alpha\,\tilde{\kappa}_{\mathrm{r}})$. These distortions result from the non-linear transfer function of low noise amplifier, band-pass filters, image rejection low pass filter, and analog-to-digital converter at the receiver. Thus, the received signal in point to point (P2P) communication under improper HWD can be modeled as

$$y = \sqrt{\alpha}x_m + \sqrt{\alpha}\eta + w; \quad m = 1, 2, \ldots, M \tag{2}$$

where $w \sim \mathcal{CN}(0, \sigma_w^2, 0)$ is the thermal noise and the aggregate effect of transceiver distortions is represented by, $\eta \sim \mathcal{CN}(0, \kappa, \tilde{\kappa})$, $\kappa = \kappa_{\mathrm{t}} + \kappa_{\mathrm{r}}$ and $\tilde{\kappa} = \tilde{\kappa}_{\mathrm{t}} + \tilde{\kappa}_{\mathrm{r}}$. Interestingly, the generalized impropriety characterization assists in accurate system modeling, rigorous performance analysis, and appropriate signaling design. Interested readers can study (Javed et al. (2020)) for the details of statistical impropriety characterization.

2.3 Noise Distribution and Optimal Receiver

Considering the aggregate noise $z = \sqrt{\alpha}\eta + w$, distributed as $z \sim CN\left(0, \alpha\kappa + \sigma_w^2, \alpha\tilde{\kappa}\right)$ where in-phase z_{I} and quadrature-phase z_{Q} noise components are distributed with the respective variances as

$$\sigma_I^2 = \left(\alpha(\kappa + \Re\left(\tilde{\kappa}\right)) + \sigma_w^2\right)/2, \tag{3}$$

$$\sigma_Q^2 = \left(\alpha(\kappa - \Re\left(\tilde{\kappa}\right)) + \sigma_w^2\right)/2, \tag{4}$$

These individual variances are obtained by simultaneously solving the equations of variance, i.e., $\mathbb{E}\left\{|z|^2\right\} = \sigma_I^2 + \sigma_Q^2$ and pseudo-variance $\mathbb{E}\left\{z^2\right\} = \sigma_I^2 - \sigma_Q^2 + 2ir_{z_I z_Q}$. Thus, the correlation $r_{z_I z_Q} = \alpha\Im\left(\tilde{\kappa}\right)/2$, defines the correlation coefficient ρ_z between z_{I} and z_{Q} as

$$\rho_z = \frac{r_{z_I z_Q}}{\sigma_I \sigma_Q} = \frac{\alpha\Im\left(\tilde{\kappa}\right)}{\sqrt{\left(\alpha\kappa + \sigma_w^2\right)^2 - \left(\alpha\Re\left(\tilde{\kappa}\right)\right)^2}}. \tag{5}$$

Unequal power distribution among quadrature noise components and non-trivial correlation coefficient marks the improper nature of aggregate additive distortions. Given the non-uniform symbol probabilities and improper noise, we propose a maximum a posterior (MAP) detector for the optimal detection as opposed to the conventional minimum Euclidean or maximum likelihood (ML) detectors (Javed et al. (2021)). Thus, the detection criterion is given by

$$\hat{m}_{\mathrm{PS}} = \underset{1 \le m \le M}{\arg\max} \quad p_X(x_m) f_{Y_{\mathrm{I}}, Y_{\mathrm{Q}}|X}\left(y_{\mathrm{I}}, y_{\mathrm{Q}}|x_m\right), \tag{6}$$

where $f_{Y_{\mathrm{I}}, Y_{\mathrm{Q}}|X}\left(y_{\mathrm{I}}, y_{\mathrm{Q}}|x_m\right)$ is the conditional Gaussian probability density function (PDF) of y given x_m derived using (Javed et al., 2020, eq. 43)

$$f_{Y_{\mathrm{I}}, Y_{\mathrm{Q}}|X}\left(y_{\mathrm{I}}, y_{\mathrm{Q}}|x_m\right) = \frac{1}{2\pi\sigma_{\mathrm{I}}\sigma_{\mathrm{Q}}\sqrt{1-\rho_z^2}} \exp\left\{\frac{-1}{2\left(1-\rho_z^2\right)}\left[\begin{array}{c} \frac{\left(y_{\mathrm{I}} - \sqrt{\alpha}\Re(x_m)\right)^2}{\sigma_{\mathrm{I}}^2} + \frac{\left(y_{\mathrm{Q}} - \sqrt{\alpha}\Im(x_m)\right)^2}{\sigma_{\mathrm{Q}}^2} + \\ - \frac{2\rho_z\left(y_{\mathrm{I}} - \sqrt{\alpha}\Re(x_m)\right)\left(y_{\mathrm{Q}} - \sqrt{\alpha}\Im(x_m)\right)}{\sigma_{\mathrm{I}}\sigma_{\mathrm{Q}}} \end{array}\right]\right\}. \tag{7}$$

3 ERROR PROBABILITY ANALYSIS

In this section, we derive the symbol error probability P_s for a system transmitting M-ary modulated symbols with prior probabilities p_m and subjected to HWD using the union bound and pairwise error probability as follows:

$$P_s \leq \sum_{m=0}^{M-1} \sum_{n \neq m} \mathrm{P}_m \Pr\left(x_m \rightarrow x_n | x_m\right). \tag{8}$$

The pairwise error probability, for receiving an erroneous symbol x_m given x_n was transmitted, can be derived using the following MAP rule,

$$\Pr\left(x_m \rightarrow x_n | x_m\right) = \Pr\left\{\mathrm{P}_m f_{Y_I,Y_Q}\left(y_I, y_Q | x_m\right) \leq \mathrm{P}_n f_{Y_I,Y_Q}\left(y_I, y_Q | x_n\right)\right\}. \tag{9}$$

Using (7) and few simplifications, we get the following bit error probability

$$P_{\mathrm{b}} \leq \mathrm{P}_{\mathrm{b}}^{\mathrm{UB}}\left(M, \alpha, \mathbf{p}\right) \triangleq \frac{1}{\log_2\left(M\right)} \sum_{m=1}^{M} \sum_{\substack{n=1\\ n \neq m}}^{M} p_m \mathcal{Q}\left(\beta_{mn}\left(\alpha\right) \ln\left(\frac{p_m}{p_n}\right) + \frac{1}{2\beta_{mn}\left(\alpha\right)}\right), \tag{10}$$

where β_{mn} is defined as

$$\beta_{mn}\left(\alpha\right) \triangleq \sqrt{\frac{\alpha^2\left(\kappa^2 - \Re\left(\tilde{\kappa}\right)^2 - \Im\left(\tilde{\kappa}\right)^2\right) + 2\alpha\kappa\sigma_w^2 + \sigma_w^4}{\alpha^2 \wp_{\mathrm{mn}} + \alpha\left(\xi_{mnI}^2 + \xi_{mnQ}^2\right) 2\sigma_w^2}}, \tag{11}$$

with $\wp_{\mathrm{mn}} = 2\xi_{mnI}^2\left(\kappa - \Re\left(\tilde{\kappa}\right)\right) + 2\xi_{mnQ}^2\left(\kappa + \Re\left(\tilde{\kappa}\right)\right) - 4\Im\left(\tilde{\kappa}\right)\xi_{mnI}\xi_{mnQ}$ while $\xi_{mn} = d_{mn} = x_m - x_n$ represents the distance between m^{th} and n^{th} symbols.

4 PROBLEM FORMULATION AND OPTIMIZATION

We propose a PS scheme, as a possible form of AS schemes, to effectively mitigate the drastic effects of additive distortions while transmitting with minimum power to minimize the EMF-exposure. To this end, we employ a higher-order M_{nu} probabilistically shaped quadrature amplitude modulation (QAM) offering more degrees of freedom and adaptive rates. The optimization problem targets the joint design of transmit power and symbol probabilities which minimize the exposure index while maintaining a throughput quality constraint. Assuming the set that includes all possible values of α as $\mathbb{A} = \{\alpha : 0 \leq \alpha \leq \alpha_{\max}\}$, we can formulate the optimization problem as

$$\mathbf{P1}: \underset{\alpha \in \mathbb{A}, \mathbf{p} \in \mathbb{S}}{\text{minimize}} \quad \mathrm{EI}\left(\alpha\right) \tag{12a}$$

$$\text{subject to} \quad \sum_{m=1}^{M_{\mathrm{nu}}} \left|x_m\right|^2 p_m \leq 1, \tag{12b}$$

$$\left(1 - \mathrm{P}_{\mathrm{b}}^{\mathrm{UB}}\left(M_{\mathrm{nu}}, \alpha, \mathbf{p}\right)\right) \mathrm{H}(\mathbf{p}) \geq \mathcal{T}_{\mathrm{u}}, \tag{12c}$$

where $\mathcal{T}_{\mathrm{u}} = \left(1 - \mathrm{P}_{\mathrm{b}}^{\mathrm{UB}}\left(M_{\mathrm{u}}, \alpha_{\max}, \mathbf{p}_{\mathrm{u}}\right)\right) \log_2\left(M_{\mathrm{u}}\right)$ is the throughput of the uniformly distributed symbol constellation with maximum power transmission. Moreover, (12b) and (12c) represent the average power and throughput QoS constraints, respectively. In addition, $\mathrm{H}(\mathbf{p})$ is the source entropy, which represents the

Algorithm 1 Alternate Optimization

```
Initialize j ← 0, ε ← ∞ and Set tolerance δ
Choose feasible starting points p^(j) and α^(j).
Evaluate EI(α^(j)).
while ε ≥ δ do
    Solve P1(a) with given α^(j) and initial point p^(j) to obtain a feasible solution p^(j*)
    Solve P1(b) given p^(j*) to obtain α^(j*)
    p^(j+1) ← p^(j*) and α^(j+1) ← α^(j*)
    Evaluate EI(α^(j+1))
    Update ε ← ‖EI(α^(j+1)) − EI(α^(j))‖
    j ← j + 1
end while
Solution parameters: p* ← p^(j+1) and α* ← α^(j+1)
Objective function: EI(α^(*))
```

transmitted rate in terms of bits per symbol per channel use and is defined as

$$\mathrm{H}(\mathbf{p}) \triangleq \sum_{m=1}^{M_{\mathrm{nu}}} -p_m \log_2\left(p_m\right). \tag{13}$$

The joint optimization problem is challenging due to the non-convex constraints. Therefore, we adopt an alternate optimization approach to iteratively solve the transmit power and symbol probabilities using the sub-problems (14) and (21), respectively. The alternate optimization Algorithm 1 begins with some initial feasible points $\mathbf{p}^{(j)}$ and $\alpha^{(j)}$ and evaluates $\mathrm{EI}\left(\alpha^{(\mathrm{j})}\right)$ for reference benchmark. Then, it finds a feasible solution of **P1(a)**, i.e., $\mathbf{p}^{(j*)}$ that satisfies (12b) and (12c). Given a probability mass function (PMF) $\mathbf{p}^{(j*)}$, we optimize **P1(b)** to minimize exposure index obtaining optimal $\alpha^{(j*)}$, which are updated to attain initial points for the next iteration. This iterative process continues until reaching an acceptable tolerance δ. Consequently, the solution parameters yield a suitable PMF and transmission power, which render a minimum exposure index while maintaining a throughput QoS.

$$\begin{aligned} \mathbf{P1(a)}: \underset{\mathbf{p}\in\mathbb{S}}{\text{find}} \quad & \mathbf{p} && (14a)\\ \text{which satisfies} \quad & (12b) \text{ and} && (14b)\\ & 1-\mathrm{P}_{\mathrm{b}}^{\mathrm{UB}}\left(M_{\mathrm{nu}},\alpha,\mathbf{p}\right) \geq \mathcal{T}_{\mathrm{u}}/\mathrm{H}(\mathbf{p}), && (14c) \end{aligned}$$

The problem **P1(a)** is a non-convex optimization problem due to the constraint (14c). Interestingly, $1/\mathrm{H}(\mathbf{p})$ is convex as the second derivative is always positive (see Appendix A). However, the bit error probability is a non-convex function in $\mathbf{p}$. Therefore, we tackle this challenge using the successive convex approximation approach based on the Taylor series approximation of the bit error probability. First-order Taylor series approximation of a function $f(x)$ around a point $x^{(k)}$ is given as

$$\tilde{f}\left(x, x^{(k)}\right) \approx f\left(x^{(k)}\right) + \nabla_x f\left(x^{(k)}\right)\left(x - x^{(k)}\right). \tag{15}$$

Thus, we need to compute $\nabla_{\mathbf{p}} \mathrm{P}_{\mathrm{b}}^{\mathrm{UB}}\left(M_{\mathrm{nu}}, \alpha, \mathbf{p}\right)$ and evaluate it at $\mathbf{p}^{(k)}$.

$$\nabla_{\mathbf{p}} \mathrm{P}_{\mathrm{b}}^{\mathrm{UB}}\left(M_{\mathrm{nu}}, \alpha, \mathbf{p}\right)=\left[\begin{array}{cccc}\frac{\partial \mathrm{P}_{\mathrm{b}}^{\mathrm{UB}}}{\partial p_1} & \frac{\partial \mathrm{P}_{\mathrm{b}}^{\mathrm{UB}}}{\partial p_2} & \ldots & \frac{\partial \mathrm{P}_{\mathrm{b}}^{\mathrm{UB}}}{\partial p_{M_{\mathrm{nu}}}}\end{array}\right]. \tag{16}$$

In order to compute $\partial \mathrm{P}_{\mathrm{b}}^{\mathrm{UB}} / \partial p_t$, we rewrite (10) as

$$\mathrm{P}_{\mathrm{b}}^{\mathrm{UB}}\left(M_{\mathrm{nu}}, \alpha, \mathbf{p}\right)=\frac{1}{\log_2\left(M_{\mathrm{nu}}\right)} \sum_{m=1}^{M_{\mathrm{nu}}} \sum_{\substack{n=1 \\ n \neq m}}^{M_{\mathrm{nu}}} p_m \int_{\Omega_{mn}}^{\infty} \frac{e^{-\frac{u^2}{2}}}{\sqrt{2\pi}} du, \tag{17}$$

where Ω_{mn} is defined as,

$$\Omega_{mn}=\beta_{mn} \ln \left(\frac{p_m}{p_n}\right)+\frac{1}{2\beta_{mn}}. \tag{18}$$

Applying the Leibniz integral rule on (17) yields the following partial derivative

$$\frac{\partial \mathrm{P}_{\mathrm{b}}^{\mathrm{UB}}}{\partial p_t} \leq \frac{1}{\log_2\left(M_{\mathrm{nu}}\right)} \sum_{\substack{n=1, \\ n \neq t, \\ m=t}}^{M_{\mathrm{nu}}}\left(\mathcal{Q}(\Omega_{mn})-\frac{\beta_{mn}}{\sqrt{2\pi}} e^{-\frac{\Omega_{mn}^2}{2}}\right)+\frac{1}{\log_2\left(M_{\mathrm{nu}}\right)} \sum_{\substack{m=1, \\ m \neq t, \\ n=t}}^{M_{\mathrm{nu}}} \frac{\beta_{mn} p_m}{\sqrt{2\pi} p_n} e^{-\frac{\Omega_{mn}^2}{2}}. \tag{19}$$

Now, $\mathrm{P}_{\mathrm{b}}^{\mathrm{UB}}\left(M_{\mathrm{nu}}, \alpha, \mathbf{p}\right)$ can be approximated from (15), (16), and (19) using first-order Taylor series expansion around an initial probability vector $\mathbf{p}^{(k)}$ as

$$\tilde{\mathrm{P}}_{\mathrm{b}}^{\mathrm{UB}}\left(M_{\mathrm{nu}}, \alpha, \mathbf{p}, \mathbf{p}^{(k)}\right) \triangleq \mathrm{P}_{\mathrm{b}}^{\mathrm{UB}}\left(M_{\mathrm{nu}}, \alpha, \mathbf{p}^{(k)}\right)+\nabla_{\mathbf{p}} \mathrm{P}_{\mathrm{b}}^{\mathrm{UB}}\left(M_{\mathrm{nu}}, \alpha, \mathbf{p}^{(k)}\right)\left(\mathbf{p}-\mathbf{p}^{(k)}\right). \tag{20}$$

Conclusively, we can solve **P1(a)** by replacing $\mathrm{P}_{\mathrm{b}}^{\mathrm{UB}}\left(M_{\mathrm{nu}}, \alpha, \mathbf{p}\right)$ in (14c) with its Taylor series approximation $\tilde{\mathrm{P}}_{\mathrm{b}}^{\mathrm{UB}}\left(M_{\mathrm{nu}}, \alpha, \mathbf{p}, \mathbf{p}^{(k)}\right)$ and solving the resultant convex feasibility problem iteratively using the well known successive convex approximation approach (Liu et al. (2019)). On the other hand, we solve **P1(b)** for a given PMF to obtain an optimal α^* which minimizes the EMF exposure.

$$\begin{aligned} \textbf{P1(b)}: \underset{\alpha \in \mathbb{A}}{\text{minimize}} \quad & \mathrm{EI}\left(\alpha\right) && (21a)\\ \text{subject to} \quad & (12c) && (21b)\end{aligned}$$

Intuitively, the throughput of probabilistically shaped M_{nu}-ary QAM is an increasing function of α because $\mathrm{P}_{\mathrm{b}}^{\mathrm{UB}}\left(M_{\mathrm{nu}}, \alpha, \mathbf{p}\right)$ is a decreasing function of α. Therefore, the solution to problem **P1(b)** is simply obtained by solving the inequality constraint with equality as

$$\mathrm{P}_{\mathrm{b}}^{\mathrm{UB}}\left(M_{\mathrm{nu}}, \alpha, \mathbf{p}\right)=1-\mathcal{T}_{\mathrm{u}} / \mathrm{H}(\mathbf{p}) \tag{22}$$

The root of the non-linear equation $\Upsilon(\alpha)=\mathrm{P}_{\mathrm{b}}^{\mathrm{UB}}\left(M_{\mathrm{nu}}, \alpha, \mathbf{p}\right)+\mathcal{T}_{\mathrm{u}} / \mathrm{H}(\mathbf{p})-1$ can be obtained using Newton-Raphson method, which begins with an initial guess $\alpha^{(j)}$ and updates it with every iteration as (Kelley (2003)),

$$\alpha^{(j+1)}=\alpha^{(j)}-\frac{\Upsilon(\alpha^{(j)})}{\Upsilon^{\prime}(\alpha^{(j)})}. \tag{23}$$

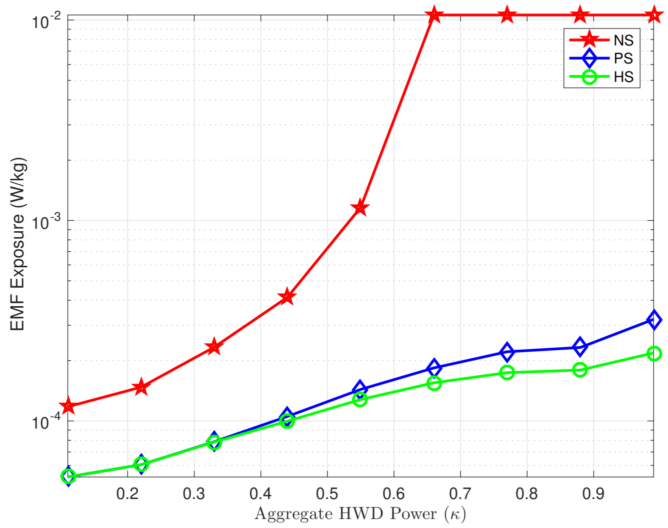

Figure 2. Exposure Index [W/kg] versus HWD power when NS transmits with $\alpha_{\max}$.

It is worthy to note that $\Upsilon'(\alpha^{(j)}) \neq 0$ and is computed from (17) as

$$\Upsilon'(\alpha) = \frac{1}{\log_2\left(M_{\text{nu}}\right)} \sum_{m=1}^{M_{\text{nu}}} \sum_{\substack{n=1 \\ n \neq m}}^{M_{\text{nu}}} p_m \frac{e^{-\Omega_{mn}^2/2}}{\sqrt{2\pi}} \left(\frac{1}{2\beta_{mn}^2} - \ln\left(\frac{p_m}{p_n}\right)\right) \frac{\partial \beta_{mn}}{\partial \alpha}, \tag{24}$$

where $\frac{\partial \beta_{mn}}{\partial \alpha}$ is expressed as

$$\frac{\partial \beta_{mn}}{\partial \alpha} = \frac{1}{2} \sqrt{\frac{\alpha^2 \wp_{\text{mn}} + \alpha\left({\xi_{mn}}_I^2 + {\xi_{mn}}_Q^2\right) 2\sigma_w^2}{\alpha^2\left(\kappa^2 - \Re\left(\tilde{\kappa}\right)^2 - \Im\left(\tilde{\kappa}\right)^2\right) + 2\alpha\kappa\sigma_w^2 + \sigma_w^4}} \text{ x} \tag{25}$$

$$\left\{ \frac{2\alpha\left(\kappa^2 - \Re\left(\tilde{\kappa}\right)^2 - \Im\left(\tilde{\kappa}\right)^2\right) + 2\kappa\sigma_w^2}{\alpha^2 \wp_{\text{mn}} + \alpha\left({\xi_{mn}}_I^2 + {\xi_{mn}}_Q^2\right) 2\sigma_w^2} - \frac{\psi(2\alpha\wp_{\text{mn}} + \left({\xi_{mn}}_I^2 + {\xi_{mn}}_Q^2\right) 2\sigma_w^2)}{(\alpha^2 \wp_{\text{mn}} + \alpha\left({\xi_{mn}}_I^2 + {\xi_{mn}}_Q^2\right) 2\sigma_w^2)^2} \right\} \tag{26}$$

with $\psi = \alpha^2\left(\kappa^2 - \Re\left(\tilde{\kappa}\right)^2 - \Im\left(\tilde{\kappa}\right)^2\right) + 2\alpha\kappa\sigma_w^2 + \sigma_w^4$. The process repeats until the desired criterion is met in terms of precision, i.e., $\Upsilon(\alpha)$ becomes acceptably small, the change is α is lesser than the predefined limit or maximum number of iterations.

5 NUMERICAL RESULTS

In this section, we present some numerical results to quantify the EMF exposure caused by the proposed PS scheme instead of the conventional no-shaping (NS). We consider an indoor active user in next-generation cellular network suffering from improper HWDs. We assume $\kappa \in \{0, 1\}$, $\rho = 0.9$, $\sigma_w^2 = 1$, $M_{\text{u}} = 8-$QAM and $M_{\text{nu}} = 16-$QAM unless specified otherwise. The reference whole-body SAR values are taken from (Vermeeren et al. (2015a), Table 27), which were computed using 3D EM simulation platforms based on the finite difference time domain and finite integration technique method. For instance, whole body SAR$^{\text{ref}}$ for standing adult is 0.0053 while for sitting is 0.0047. On the other hand, for child it is 0.015 and 0.014,

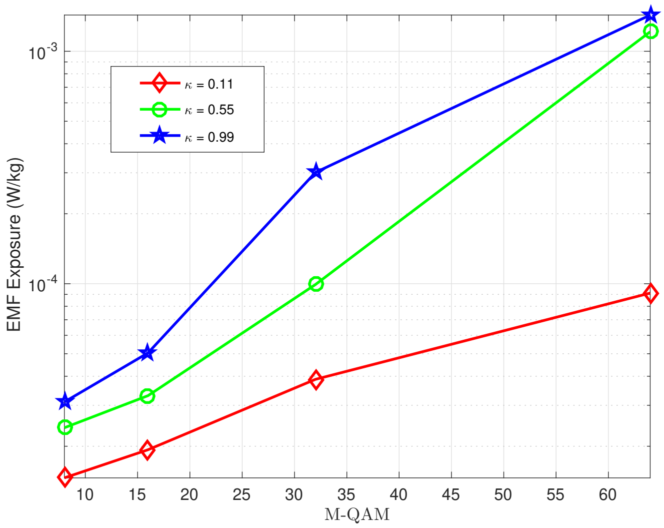

Figure 3. Exposure Index [W/kg] versus modulation order

respectively, for the uplink voice communication at 2.6 GHz frequency band. In number results, we take the average reference SAR weighted by the number of users in each category along with their respective postures. In particular, we consider $\mathrm{SAR}^{\mathrm{ref}} = 41\mathrm{x}10^{-4}$ W/Kg for data users and $\mathrm{SAR}^{\mathrm{ref}} = 63\mathrm{x}10^{-4}$ W/Kg for voice users per unit power (Ibraiwish et al. (2022)). Evidently, the SAR reference value of voice users is higher as compared to the data users because the voice users are expected to keep the cellular mobile phones near their brains.

At first, we investigate the EMF exposure of a single active user for a range of HWD levels. We present the comparison between the traditional NS scheme employing $M_{\mathrm{u}}-$QAM and the proposed PS scheme employing $M_{\mathrm{nu}}-$QAM. For a fair comparison, we minimize the exposure index of M_{u}-QAM with uniform distribution $\mathbf{p_u}$ (NS) scheme to ensure a throughput threshold of $\mathcal{T}_0 = 2.997$ bits/sec, i.e.,

$$\mathbf{P2(a)}: \underset{\alpha_{\mathrm{u}} \in \mathbb{A}}{\text{minimize}} \quad \mathrm{EI}\left(\alpha_{\mathrm{u}}\right) \tag{27a}$$

$$\text{subject to} \quad \left(1 - \mathrm{P}_{\mathrm{b}}^{\mathrm{UB}}\left(M_{\mathrm{u}}, \alpha, \mathbf{p_u}\right)\right) \log_2(M_{\mathrm{u}}) \geq \mathcal{T}_0, \tag{27b}$$

The simulation results provide the insights of the Exposure Index of no-shaping versus probabilistic shaping for a range of HWD to achieve a target throughput, as shown in Figure 2. Evidently, they reveal the superiority of employing PS to successfully limit the EMF exposure while maintaining the QoS in terms of throughput. The advantage of PS over NS is particularly prominent for higher distortion levels. Moreover, we move a step further to investigate the performance of the HS scheme with $M_{\mathrm{nu}}-$QAM employing an aggregate of GS and PS as detailed in Javed et al. (2021). Interestingly, HS reduces the EMF exposure for higher distortion levels but the gain is insignificant given the added complexity in designing GS and PS parameters. Conclusively, PS is the preferred choice as it can reduce EMF exposure up to 98% with affordable complexity.

Next, we study the impact of varying the modulation order for three different distortion levels on the EMF exposure in Figure 3. We assumed modulation order M_{nu} ranging from 8-QAM to 64-QAM for the proposed PS. Noticeably, the increasing modulation order increases the EMF exposure for all HWD levels,

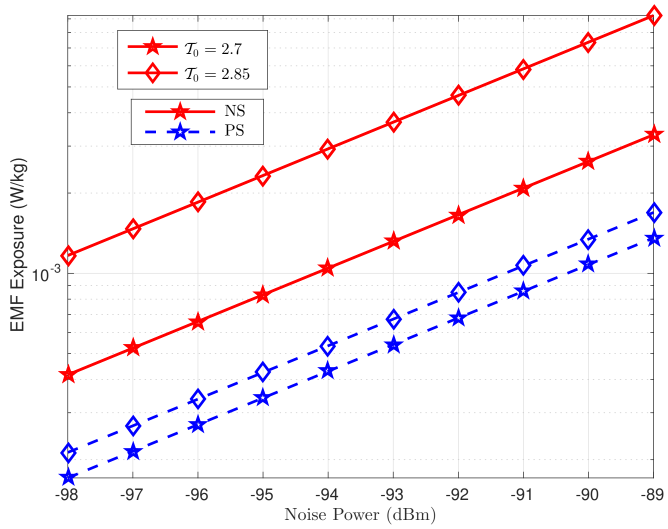

Figure 4. Exposure Index [W/kg] versus noise variance.

i.e., least, medium and high distortion levels, however, at different paces. Intuitively, more transmit power is required to meet the QoS constraint in a highly distorted system instead of the least distorted system, which advocates a considerable EMF exposure of higher distortion levels.

Similarly, we analyzed the benefits of PS over NS for a range of noise variance (-98dBm to -89dBm) for two different target throughputs, i.e., $\mathcal{T}_0 = 2.7$ bits/sec and $\mathcal{T}_0 = 2.85$ bits/sec. We can observe a 55% and 81.82% percent reduction in EMF exposure at -98dBm for the target threshold rates of 2.7 and 2.85 bits per sec per channel, respectively, with PS over NS as shown in Figure 4. Intuitively, PS outperforms NS for the entire range of noise variance in decreasing the EMF exposure on a user.

6 CONCLUSION

Throughout this paper, we highlight the significance of employing probabilistic shaping (PS) to mitigate the drastic effects of improper hardware distortions and effectively reduce the user's EMF exposure while maintaining a target threshold. The numerical results reveal up to a 98% percentage reduction in Exposure Index with the help of PS as compared to the conventional NS. Further investigation demonstrates a minor gain with HS over PS with significant added complexity. Thus, we conclude that mere PS is the preferred choice to reduce the exposure index, given a trade-off between lowering EI and increasing computational complexity.

DATA AVAILABILITY STATEMENT

The original contributions of this work are presented in the article/Supplementary Material, further inquiries can be directed to the corresponding author.

AUTHOR CONTRIBUTIONS

The study was conducted as a collaboration among all authors. AE conceived the work. The manuscript was mainly drafted by SJ and was revised and approved by all co-authors.

APPENDIX A: PROOF OF CONVEXITY

The first and second order derivatives of $1/\mathrm{H}(\mathbf{p})$ are given as

$$\nabla_{\mathbf{p}} \left(1/\mathrm{H}(\mathbf{p})\right) = -\mathrm{H}'(\mathbf{p})/\left[\mathrm{H}(\mathbf{p})\right]^2 \tag{28}$$

$$\nabla^2_{\mathbf{p}} \left(1/\mathrm{H}(\mathbf{p})\right) = -\frac{\left[\mathrm{H}(\mathbf{p})\right]^2 \mathrm{H}''(\mathbf{p}) - 2\left[\mathrm{H}'(\mathbf{p})\right]^2 \mathrm{H}(\mathbf{p})}{\left[\mathrm{H}(\mathbf{p})\right]^4} \geq 0 \quad \because \quad \mathrm{H}(\mathbf{p}) \geq 0 \text{ and } \mathrm{H}''(\mathbf{p}) \leq 0 \tag{29}$$

The second order derivative is always positive given the non-negative and concave nature of information entropy. Hence, we can safely conclude that $1/\mathrm{H}(\mathbf{p})$ is a convex function in $\mathbf{p}$.

REFERENCES

Bhushan, N., Li, J., Malladi, D., Gilmore, R., Brenner, D., Damnjanovic, A., et al. (2014). Network densification: the dominant theme for wireless evolution into 5G. *IEEE Communications Magazine* 52, 82–89

Björnson, E., Hoydis, J., Kountouris, M., and Debbah, M. (2014). Massive MIMO systems with non-ideal hardware: Energy efficiency, estimation, and capacity limits. *IEEE Trans. Inf. Theory* 60, 7112–7139

Björnson, E., Matthaiou, M., and Debbah, M. (2013). A new look at dual-hop relaying: Performance limits with hardware impairments. *IEEE Trans. Commun.* 61, 4512–4525

Boulogeorgos, A.-A. A., Chatzidiamantis, N. D., and Karagiannidis, G. K. (2016). Energy detection spectrum sensing under RF imperfections. *IEEE Trans. Commun.* 64, 2754–2766

[Dataset] Buchner, K. and Rivasi, M. (2020). The international commission on non-ionizing radiation protection: Conflicts of interest, corporate capture and the push for 5G

Chiaraviglio, L., Elzanaty, A., and Alouini, M.-S. (2021). Health risks associated with 5G exposure: A view from the communications engineering perspective. *IEEE Open Journal of the Communications Society* 2, 2131–2179. doi:10.1109/OJCOMS.2021.3106052

Duy, T. T., Duong, T. Q., da Costa, D. B., Bao, V. N. Q., and Elkashlan, M. (2015). Proactive relay selection with joint impact of hardware impairment and co-channel interference. *IEEE Trans. Commun.* 63, 1594–1606

Elzanaty, A., Chiaraviglio, L., and Alouini, M.-S. (2021). 5G and EMF exposure: Misinformation, open questions, and potential solutions. *Front. Comms. Net.* 2, 5. doi:10.3389/frcmn.2021.635716

[Dataset] Elzanaty, A. M. and Alouini, M.-S. (2022). Communicating over a free-space optical channel using distribution matching. US Patent App. 17/357,450

Group, I. W. (2013). *Non-ionizing radiation, Part 2: Radiofrequency electromagnetic fields*. Tech. rep., International Agency for Research on Cancer (IARC) Working Group on the Evaluation of Carcinogenic Risks to Humans. Vol. 102

Ibraiwish, H., Elzanaty, A., Al-Badarneh, Y. H., and Alouini, M.-S. (2022). EMF-aware cellular networks in RIS-assisted environments. *IEEE Commun. Lett.* 26, 123–127. doi:10.1109/LCOMM.2021.3120688

Javed, S., Amin, O., Ikki, S. S., and Alouini, M.-S. (2017). Asymmetric hardware distortions in receive diversity systems: Outage performance analysis. *IEEE Access* 5, 4492–4504

Javed, S., Amin, O., Shihada, B., and Alouini, M.-S. (2019). Improper Gaussian signaling for hardware impaired multihop full-duplex relaying systems. *IEEE Trans. Commun.* 67, 1858–1871

Javed, S., Amin, O., Shihada, B., and Alouini, M.-S. (2020). A journey from improper Gaussian signaling to asymmetric signaling. *IEEE Communications Surveys Tutorials* 22, 1539–1591. doi:10.1109/COMST.2020.2989626

Javed, S., Elzanaty, A., Amin, O., Shihada, B., and Alouini, M.-S. (2021). When probabilistic shaping realizes improper signaling for hardware distortion mitigation. *IEEE Trans. Commun.*

Kelley, C. T. (2003). *Solving nonlinear equations with Newton's method* (SIAM)

Kuehn, S., Pfeifer, S., Kochali, B., Kuster, N., and Bern, C. (2019). Modelling of total exposure in hypothetical 5G mobile networks for varied topologies and user scenarios. *Final Report of Project CRR* 816

Latva-aho, M., Leppänen, K., Clazzer, F., and Munari, A. (2020). Key drivers and research challenges for 6G ubiquitous wireless intelligence

Liu, A., Lau, V. K., and Kananian, B. (2019). Stochastic successive convex approximation for non-convex constrained stochastic optimization. *IEEE Trans. Signal Processing* 67, 4189–4203

Lou, Z., Elzanaty, A., and Alouini, M.-S. (2021). Green tethered UAVs for EMF-aware cellular networks. *IEEE Trans. Green Commun. Netw.* doi:10.1109/TGCN.2021.3102086

Matalatala, M., Deruyck, M., Tanghe, E., Martens, L., and Joseph, W. (2018). Optimal low-power design of a multicell multiuser massive MIMO system at 3.7 GHz for 5G wireless networks. *Wireless Communications and Mobile Computing* 2018

National Toxicology Program (2018a). *Toxicology and carcinogenesis studies in B6C3F1/N mice exposed to whole-body radio frequency radiation at a frequency (1,900 MHz) and modulations (GSM and CDMA) used by cell phones*. Tech. rep., NTO

National Toxicology Program (2018b). *Toxicology and Carcinogenesis Studies in Hsd: Sprague Dawley SD Rats Exposed to Whole-Body Radio Frequency Radiation at a Frequency (900 MHz) and Modulations (GSM and CDMA) Used by Cell Phones*. Tech. rep., NTO

Santamaria, I., Crespo, P. M., Lameiro, C., and Schreier, P. J. (2018). Information-theoretic analysis of a family of improper discrete constellations. *Entropy* 20, 45

Schenk, T. (2008). *RF imperfections in high-rate wireless systems: Impact and digital compensation* (Springer Science & Business Media)

Studer, C., Wenk, M., and Burg, A. (2010). MIMO transmission with residual transmit-RF impairments. In *Proc. Int. ITG Workshop on Smart Antennas (WSA)* (Bremen, Germany: IEEE), 189–196

Suzuki, H., Tran, T. V. A., Collings, I. B., Daniels, G., and Hedley, M. (2008). Transmitter noise effect on the performance of a MIMO-OFDM hardware implementation achieving improved coverage. *IEEE Journal on Selected Areas in Commun.* 26, 867–876

Tesanovic, M., Conil, E., De Domenico, A., Aguero, R., Freudenstein, F., Correia, L. M., et al. (2014). The LEXNET project: Wireless networks and EMF: Paving the way for low-EMF networks of the future. *IEEE Vehicular Technology Magazine* 9, 20–28

Vermeeren, G., Plets, D., Joseph, W., Martens, L., Oliveira, C., Sebastião, D., et al. (2015a). *Low EMF Exposure Future Networks D2. 8 Global Wireless Exposure Metric Definition*. Tech. rep.

Vermeeren, G., Plets, D., Joseph, W., Martens, L., Oliveira, C., Sebastião, D., et al. (2015b). *Low EMF exposure future networks D2. 8 global wireless exposure metric definition*. Tech. rep., LEXNET project deliverable

Vornoli, A., Falcioni, L., Mandrioli, D., Bua, L., and Belpoggi, F. (2019). The contribution of in vivo mammalian studies to the knowledge of adverse effects of radiofrequency radiation on human health. *International Journal of Environmental Research and Public Health* 16. doi:10.3390/ijerph16183379

Wan, L., Guo, Z., Wu, Y., Bi, W., Yuan, J., Elkashlan, M., et al. (2018). 4G/5G spectrum sharing: Efficient 5G deployment to serve enhanced mobile broadband and internet of things applications. *IEEE Vehicular Technology Magazine* 13, 28–39. doi:10.1109/MVT.2018.2865830

Wenk, M. (2010). *MIMO-OFDM-testbed: challenges, implementations, and measurement results* (ETH Zurich)

Wilbourn, J., Haroun, L., Heseltine, E., Kaldor, J., Partensky, C., and Vainio, H. (1986). Response of experimental animals to human carcinogens: an analysis based upon the IARC monographs programme. *Carcinogenesis* 7, 1853–1863

Xia, X., Zhang, D., Xu, K., Ma, W., and Xu, Y. (2015). Hardware impairments aware transceiver for full-duplex massive MIMO relaying. *IEEE Trans. Signal Process.* 63, 6565–6580

Zetterberg, P. (2011). Experimental investigation of TDD reciprocity-based zero-forcing transmit precoding. *EURASIP J. Adv. Signal Process.* 2011, 5